The highly deformed nucleus ^{40}Ca in the fusionlike deformation valley

G. Royer and C. Bonilla
Laboratoire Subatech, UMR: IN2P3/CNRS-Université-Ecole des Mines, 4 rue A. Kastler, F-44307 Nantes Cedex 03, France

R. A. Gherghescu
National Institute for Physics and Nuclear Engineering, P.O. Box MG-6, RO-76900 Bucharest, Romania

(Received 26 March 2002; published 10 June 2002)

The potential barriers governing the evolution of the doubly magic nucleus ^{40}Ca have been determined within a rotating liquid drop model including a proximity energy term, the two-center shell model, and the Strutinsky method. In addition to the quasispherical ground state, the macromicroscopic deformation and rotational energies generate a second highly deformed minimum where superdeformed and highly deformed states may survive. The predicted characteristics roughly agree with the recently observed data on superdeformed rotational bands in ^{40}Ca.

DOI: 10.1103/PhysRevC.65.067304 PACS number(s): 25.70.Jj, 21.60.Ev, 21.60.Cs

Superdeformed rotational bands have been observed recently [1] in ^{40}Ca. The high spin states were populated via the reaction ^{28}Si(^{20}Ne,2α)^{40}Ca with an effective beam energy of 80 MeV. The measured quadrupole moment for transition between states with spin from $16\hbar$ to $2\hbar$ is $1.80^{+0.39}_{-0.29}$ e b; the excitation energy varying from 22.1 MeV to 5.6 MeV and the moment of inertia being around $8\hbar^2$ MeV^{-1}. Superdeformed rotational states have been also observed in neighboring nuclei ^{36}Ar [2] and ^{56}Ni [3] as well as highly deformed bands in ^{56}Ni [3,4], ^{65}Zn [5], ^{130}Nd [6], and ^{152}Dy [7].

In the present study the purpose is to determine the l-dependent potential barriers governing the evolution of a rotating doubly magic nucleus ^{40}Ca within a macromicroscopic energy. Within such an approach, shape sequences must be selected. The geometrical characteristics deduced from the experimental data (mainly the moment of inertia and quadrupole moment) are not sufficient to unambiguously discriminate between the different possible shape sequences. Nevertheless, for light nuclear systems, most studies conclude that the compound nucleus scission and saddle shapes look like two close, almost spherical fragments. Consequently, a quasimolecular shape already defined to describe the fusion valley [8] has been retained. In this shape sequence, the deformation path leads from the sphere to two tangent spherical nuclei assuming the rapid formation of a deep neck in a one-body compact shape while keeping almost spherical ends; the two spherical fragments going away later.

The macroscopic deformation energy has been calculated within a generalized liquid drop model (GLDM) taking into account both the proximity energy in the neck or the gap between the fragments and an accurate radius. The shell effects have been derived within two approaches. The first one uses the two-center shell model and the Strutinsky method [9]. The second one is a simpler algebraic approach derived from the droplet model formulas [10,11] and from an idea and microscopic calculations of Nörenberg [12] according to which the nuclear interaction responsible for the proximity energy in the neck strongly mixes and perturbs the single-particle states and therefore weakens the shell effects.

The validity of the combination of this GLDM and quasimolecular shapes has been proved by its efficiency to reproduce reasonably well most of the fusion [8], fission [11,13], cluster [14], and α [15] emission data without changing the parameters. As an example, the barrier height for the evaporation of α particles from the rotating compound nucleus ^{200}Pb at $22\hbar$ mean angular momentum has been determined recently [16] experimentally as being 18.0 MeV. The GLDM gives 16.8 MeV while the standard optical model leads to 20.1 MeV. Vaz and Alexander [17] obtained, respectively, 19.9 and 17.4 MeV for cold and hot nuclei.

In this fusionlike deformation valley, the barrier top corresponds to two-body configurations and the selected one-body shape sequence does not play a main role to determine the barrier height. This justifies the use of a one parameter dependent shape sequence.

Within this GLDM [8] the macroscopic energy of a deformed nucleus is defined as

$$E = E_V + E_S + E_C + E_N + E_{rot}. \tag{1}$$

For one-body shapes, the volume E_V, surface E_S and Coulomb E_C energies are given by

$$E_V = -15.494(1-1.8I^2)A \ \text{MeV}, \tag{2}$$

$$E_S = 17.9439(1-2.6I^2)A^{2/3}(S/4\pi R_0^2) \ \text{MeV}, \tag{3}$$

$$E_C = 0.6e^2(Z^2/R_0)\times 0.5\int [V(\theta)/V_0][R(\theta)/R_0]^3 \sin\theta d\theta. \tag{4}$$

S is the surface of the one-body deformed nucleus and I is the relative neutron excess. $V(\theta)$ is the electrostatic potential at the surface and V_0 the surface potential of the sphere.

For separated spherical fragments

$$E_{V12} = -15.494[(1-1.8I_1^2)A_1 + (1-1.8I_2^2)A_2] \ \text{MeV}, \tag{5}$$

$$E_{S12} = 17.9439[(1-2.6I_1^2)A_1^{2/3} + (1-2.6I_2^2)A_2^{2/3}] \ \text{MeV}, \tag{6}$$

$$E_{C12}=0.6e^2Z_1^2/R_1+0.6e^2Z_2^2/R_2+e^2Z_1Z_2/r, \qquad (7)$$

where A_i, Z_i, R_i, and I_i are the masses, charges, radii, and relative neutron excesses of the fragments; r being the distance between the mass centres.

The radius R_0 of the parent nucleus has been chosen as

$$R_0=(1.28A^{1/3}-0.76+0.8A^{-1/3}) \text{ fm}. \qquad (8)$$

This later formula often used only to determine the proximity energy allows one to take into account the experimentally observed increase of the ratio $r_0=R_0/A^{1/3}$ with the mass; for example, $r_0=1.126$ fm for ^{40}Ca. The radius of the fragments is determined assuming volume conservation.

For comparison, in the RLDM and RFRM approaches [18,19] the reduced radius r_0 is, respectively, 1.225 fm and 1.16 fm with no mass dependence while the surface coefficient a_s takes the values 17.94 MeV and 21.13 MeV.

The surface energy term E_S takes into account only the surface tension forces in a half space and does not include the contribution due to the attractive nuclear forces between the surfaces considered in a neck or a gap between separated fragments. The nuclear proximity energy term E_N allows one to take into account these additional surface effects when a neck or a gap appears. This term is essential to describe smoothly the one-body to two-body transition via quasimolecular shapes. For example, at the contact point between two spherical ^{20}Ne nuclei the proximity energy reaches -22.2 MeV,

$$E_N(r)=2\gamma\int_{h_{min}}^{h_{max}}\Phi[D(r,h)/b]2\pi h dh. \qquad (9)$$

h is the transverse distance varying from the neck radius or zero to the height of the neck border. D is the distance between the opposite surfaces in consideration and b the surface width fixed at 0.99 fm. Φ is the proximity function. The surface parameter γ is the geometric mean between the surface parameters of the two fragments:

$$\gamma=0.9517\sqrt{(1-2.6I_1^2)(1-2.6I_2^2)} \text{ MeV fm}^{-2}. \qquad (10)$$

In this GLDM the surface diffuseness is not taken into account and the proximity energy vanishes when there is no neck as for an ellipsoid for example.

All along the deformation path the rotational energy has been determined within the rigid body ansatz

$$E_{rot}=\hbar^2 l(l+1)/2I_\perp . \qquad (11)$$

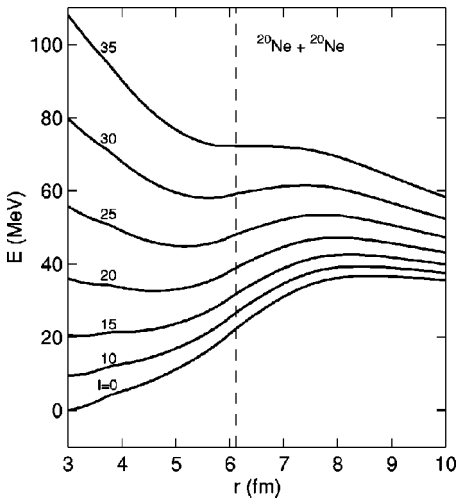

FIG. 1. For symmetric deformations of ^{40}Ca, sum of the macroscopic deformation and rotational energies as functions of the angular momentum ($\hbar$ unit) and the distance r between the mass centers. The vertical dashed line indicates the separation into two spherical nuclei.

Indeed, it has been shown that corrective terms arising from the orbital motion and the spin degrees of freedom roughly cancel each other, particularly at large deformations.

The l-dependent macroscopic potential barriers against symmetric decay are displayed in Fig. 1 for the ^{40}Ca nucleus. The macroscopic barriers for the ^{152}Dy, ^{56}Ni, and ^{48}Cr nuclei have been previously studied [20,21].

In all cases the proximity energy introduces an inflection in the potential energy curve preventing the separation of the nascent fragments. The two tangent sphere configuration is reached before crossing the barrier, the top of which corresponding to two separated spheres maintained in unstable equilibrium by the balance between the attractive nuclear forces and the repulsive Coulomb ones. The centrifugal forces can remove these potential pockets only for very high angular momenta due to the high curvature and high values of the moment of inertia at the barrier top.

In the successfull experiment [1] the chosen beam energy allowed one to pass the l-dependent fusion barriers until $30\hbar-35\hbar$ and consequently to populate all the states present in the potential wells. To determine the most suitable beam energy and to calculate the fusion cross sections, analytical formulas have been proposed recently [22] for the fusion barrier heights $E_{fus,l=0}$ and positions $R_{fus,l=0}$.

$$E_{fus,l=0} \text{ (MeV)}=-19.38+\frac{2.1388Z_1Z_2+59.427(A_1^{1/3}+A_2^{1/3})-27.07\ln\left(\frac{Z_1Z_2}{A_1^{1/3}+A_2^{1/3}}\right)}{(A_1^{1/3}+A_2^{1/3})[2.97-0.12\ln(Z_1Z_2)]}, \qquad (12)$$

$$R_{fus,l=0} \text{ (fm)}=(A_1^{1/3}+A_2^{1/3})\left[1.908-0.0857\ln(Z_1Z_2)+\frac{3.94}{Z_1Z_2}\right]. \qquad (13)$$

They reproduce accurately the GLDM predictions and the experimental data. Here a new formula that gives the *l*-dependent fusion barrier heights is proposed.

$$E_{fus,l}\ (\mathrm{MeV}) = E_{fus,l=0} + \frac{l(l+1)}{0.02081(A_1^{5/3}+A_2^{5/3}) + \dfrac{0.0506 A_1 A_2 (A_1^{1/3}+A_2^{1/3})^2 \left(1.908 + \dfrac{3.94}{Z_1 Z_2} - 0.0857 ln(Z_1 Z_2)\right)^2}{A_1+A_2}}. \quad (14)$$

The added term corresponds to the increase of the energy at the barrier top due to the rotational energy. The moment of inertia corresponds to two separated spheres and the two coefficients have been adjusted to take into account the shifting of the barrier to inner positions. The accuracy of this formula is correct for light nuclei and very good for heavy elements.

The macromicroscopic potential barriers obtained by adding the shell corrections given by the two-center shell model and the Strutinsky method [9] at the *l*-dependent macroscopic energy are displayed in Fig. 2. An adjustment has also been done to reproduce the experimental *Q* value with a corrective factor ending at the contact point between the nascent touching fragments. These shell effects generate a high hump relatively close to the sphere and consequently a second deformed minimum appears even at $l=0$. The first minimum remains even at high angular momenta but the second minimum becomes the lowest one around $17\hbar$. The calculated quadrupole moment for transition between states with spins from $16\hbar$ to $2\hbar$ varies from $2.5^{+0.4}_{-0.3}$ *e* b at $16\hbar$ to $2.2^{+0.3}_{-0.3}$ *e* b at $2\hbar$. The moment of inertia evolves from $9.7^{+0.8}_{-0.7}\hbar^2$ MeV^{-1} to $9.1^{+0.6}_{-0.6}\hbar^2$ MeV^{-1} and the excitation energy from 23.9 MeV to 9.7 MeV. The limits of the uncertainty range correspond to the geometric characteristics of the deformed nuclei located in the second potential pocket and having an energy of 0.4 MeV above the energy of the second minimum present in this external well.

As a matter of fact, the behavior of the shell effects at large deformations is very poorly known even for one-body shapes. For quasimolecular shapes and particularly at the rupture point of the matter bridge between the fragments, it is questionable to speak about nuclear orbits when there is an exchange of nucleons between these fragments to equilibrate the mass and charge distributions. Therefore the macromicroscopic potential barriers shown in Fig. 3 have been determined on the assumption that the shell effects vanish around the contact point. The shell effects given by the algebraic approach of the droplet model [10,11] have been added, for one-body shapes, at the macroscopic energy given by the GLDM. They vanish relatively rapidly and at $l=0$ there is a plateau but not deep second minimum. The first minimum around the sphere disappears at the highest angular momenta. With increasing angular momentum, a second highly deformed minimum appears. It becomes the lowest one also around $17\hbar$. Its precise location is due to the shell effects but the underlying macroscopic energy plays also an important role, particularly the inflection in the curve due to the proximity energy. The calculated quadrupole moment for transition between states with spins from $16\hbar$ to $2\hbar$ varies then from $2.3^{+0.5}_{-0.4}$ *e* b at $16\hbar$ to $1.8^{+0.3}_{-0.6}$ *e* b at $2\hbar$. The moment of inertia evolves from $9.4^{+1.0}_{-0.8}\hbar^2$ MeV^{-1} to $8.3^{+0.6}_{-1.1}\hbar^2$ MeV^{-1} and the excitation energy from 24.3 MeV to 9.0 MeV. These results agree with the experimental data recently obtained on this nucleus except for the excitation energy at $2\hbar$ which is too large. After the separation point, the shell effects coming

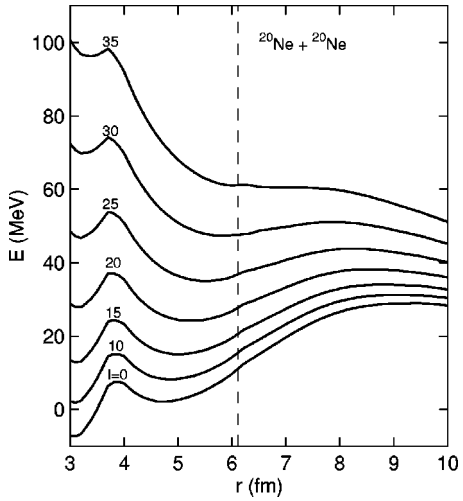

FIG. 2. Same as Fig. 1 but the shell effects calculated within the two-center shell model and the Strutinsky method are added and the experimental *Q* value is taken into account.

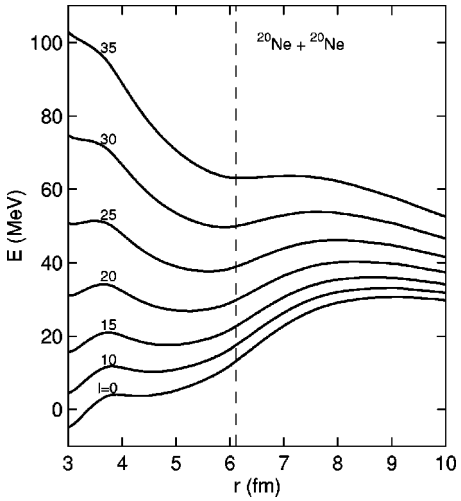

FIG. 3. Same as Fig. 1 but the shell effects calculated within an algebraic approach [10] are added and the experimental *Q* value is taken into account.

from the two fragments have been introduced progressively starting from zero at the contact point to reach the full value at 3 fm beyond the contact point. These shell corrections at the barrier top do not play an important role to stabilize the highly deformed system except for the highest angular momenta.

In summary, the potential barriers governing the evolution of a rotating nucleus ^{40}Ca have been determined using a generalized liquid drop model including the nuclear proximity energy and quasimolecular shapes; the shell effects being calculated within the two center shell model and, alternatively, with an algebraic approach derived from the droplet model. The appearance of the second deformed minimum with increasing angular momentum and the disappearance of the well around the sphere are sensitive to the prescription used to determine the shell effects. At intermediate spins, both the shell corrections and the proximity energy contribute to form the second potential pocket while, for the highest spins, the persistence of a highly deformed minimum is mainly due to the proximity forces that prevent the negotiating of the scission barrier.

The results for the quadrupole moment, the moment of inertia, and the excitation energy agree roughly with the data obtained recently on the superdeformed rotational bands in ^{40}Ca, the predicted excitation energy for the lowest spins being somewhat too large. New experiments are desirable to test the predictions of highly deformed states at very high spins.

[1] E. Ideguchi *et al.*, Phys. Rev. Lett. **87**, 222501 (2001).
[2] C. E. Svensson *et al.*, Phys. Rev. C **63**, 061301(R) (2001).
[3] D. Rudolph *et al.*, Phys. Rev. Lett. **82**, 3763 (1999).
[4] C. Bhattacharya *et al.*, Nucl. Phys. **A654**, 841c (1999).
[5] C.-H. Yu *et al.*, Phys. Rev. C **62**, 041301(R) (2000).
[6] D. J. Hartley *et al.*, Phys. Rev. C **63**, 024316 (2001).
[7] A. Galindo-Uribarri *et al.*, Phys. Rev. Lett. **71**, 231 (1993).
[8] G. Royer and B. Remaud, Nucl. Phys. **A444**, 477 (1985).
[9] R. A. Gherghescu and G. Royer, Int. J. Mod. Phys. E **9**, 51 (2000).
[10] W. D. Myers, *Droplet Model of Atomic Nuclei* (Plenum, New York, 1977).
[11] G. Royer and B. Remaud, J. Phys. G **10**, 1057 (1984).
[12] W. Nörenberg, Phys. Rev. C **5**, 2020 (1972).
[13] G. Royer and K. Zbiri, Nucl. Phys. **A697**, 630 (2002).
[14] G. Royer, R. Moustabchir, Nucl. Phys. **A683**, 182 (2001).
[15] G. Royer, J. Phys. G **26**, 1149 (2000).
[16] G. Viesti *et al.*, Phys. Lett. B **521**, 165 (2001).
[17] L. C. Vaz and J. M. Alexander, Z. Phys. A **318**, 231 (1984).
[18] A. J. Sierk, Phys. Rev. Lett. **55**, 582 (1985).
[19] A. J. Sierk, Phys. Rev. C **33**, 2039 (1986).
[20] G. Royer and F. Haddad, Phys. Rev. C **47**, 1302 (1993).
[21] G. Royer, J. Phys. G **21**, 249 (1995).
[22] R. Moustabchir and G. Royer, Nucl. Phys. **A683**, 266 (2001).